TISSUE ENGINEERING: Part A Volume 24, Numbers 7 and 8, 2018 © Mary Ann Liebert, Inc. DOI: 10.1089/ten.tea.2017.0153



ORIGINAL ARTICLE

Wnt/Yes-Associated Protein Interactions During Neural Tissue Patterning of Human Induced Pluripotent Stem Cells

Julie Bejoy, MS, Liqing Song, MS, Yi Zhou, PhD, and Yan Li, PhD 1

Human induced pluripotent stem cells (hiPSCs) have special ability to self-assemble into neural spheroids or minibrain-like structures. During the self-assembly process, Wnt signaling plays an important role in regional patterning and establishing positional identity of hiPSC-derived neural progenitors. Recently, the role of Wnt signaling in regulating Yes-associated protein (YAP) expression (nuclear or cytoplasmic), the pivotal regulator during organ growth and tissue generation, has attracted increasing interests. However, the interactions between Wnt and YAP expression for neural lineage commitment of hiPSCs remain poorly explored. The objective of this study is to investigate the effects of Wnt signaling and YAP expression on the cellular population in three-dimensional (3D) neural spheroids derived from hiPSCs. In this study, Wnt signaling was activated using CHIR99021 for 3D neural spheroids derived from human iPSK3 cells through embryoid body formation. Our results indicate that Wnt activation induces nuclear localization of YAP and upregulates the expression of HOXB4, the marker for hindbrain/spinal cord. By contrast, the cells exhibit more rostral forebrain neural identity (expression of TBR1) without Wnt activation. Cytochalasin D was then used to induce cytoplasmic YAP and the results showed the decreased HOXB4 expression. In addition, the incorporation of microparticles in the neural spheroids was investigated for the perturbation of neural patterning. This study may indicate the bidirectional interactions of Wnt signaling and YAP expression during neural tissue patterning, which have the significance in neurological disease modeling, drug screening, and neural tissue regeneration.

Keywords: pluripotent stem cell, neural patterning, Wnt, YAP, three-dimensional

Introduction

HUMAN PLURIPOTENT STEM CELLS (hPSCs) are able to self-assemble into three-dimensional (3D) organoids that have the organized structure that in part recapitulate human tissue morphogenesis. In particular, mini-brains derived from hPSCs display distinct regions that are identifiable for forebrain, midbrain, and hindbrain layers. Similarly, the forebrain cortical spheroids or organoids derived from human induced pluripotent stem cells (hiPSCs) show the layer-specific structure that is similar to human cortex. These studies are significant to enable the access to human brain-like tissue and recapitulate the genetic neurological diseases such as microcephaly, Alzheimer's disease, and amyotrophic lateral sclerosis for pathological and virus infection study. In addition, these 3D neural constructs provide

a novel platform for drug screening that provides the physiologically relevant human brain tissue models.^{2,9}

During the hiPSC self-assembly process, the influence of biochemical signaling on the brain tissue structure development has been poorly understood. Most current strategies are to let hiPSC self-organize in the presence of a differentiation medium. This approach provides little guidance and prediction on the structure and the specific region of the brain tissues or organoids derived from hiPSCs. In addition, the procedure is very long, lasting from 50 days up to 140 days. All these facts motivate advanced understanding of the extrinsic factors and intrinsic signaling pathways to influence neural tissue patterning from hiPSCs.

Wnt signaling is one of the major pathways that influence coordinated proliferation and differentiation during organ growth and serves as extrinsic signaling to regulate stem cell

¹Department of Chemical and Biomedical Engineering, FAMU-FSU College of Engineering, Florida State University, Tallahassee, Florida.

²Department of Biomedical Sciences, College of Medicine, Florida State University, Tallahassee, Florida.

The preliminary results of this study were presented in the 2016 Annual Meeting of American Institute of Chemical Engineers (AIChE), November 13–18, San Francisco, CA, 2016.

fate decisions during tissue development and regeneration.¹¹ The most known Wnt pathway is the canonical Wnt/β-catenin signaling. Under Wnt activation, Wnt protein attaches to its receptor(s) at cell membrane and cause β-catenin translocation into the nucleus, which regulates the transcription of Wnt target genes by binding to T-cell factor/lymphoid enhancer factor. The novel role of Wnt signaling in neural differentiation of hPSCs has drawn attentions recently. 14,15 For example, Wnt signaling was found to regulate neural differentiation along rostral (Wnt low) and caudal (Wnt high) identity when Wnt was increased from a low to high level, resulting in different cellular composition of hPSC-derived neural progenitor cells (NPCs). 15 Wnt activation supplemented with retinoic acid (RA) and ventralization factor Sonic Hedgehog also promoted motor neuron differentiation from hPSCs, showing caudalization effect. 14,16 However, the influence of Wnt signaling on spatial patterning of neural populations from hPSCs in 3D culture has not been well understood.

Moreover, Wnt pathway impacts Hippo/Yes-associated protein (YAP) signaling in organ growth and size control. 17,18 YAP/transcriptional coactivator with PDZ-binding motif (TAZ) and β-catenin can form destruction complex and modulate cellular response to Wnt signaling. 19 YAP/TAZ may also affect Wnt signaling through an alternative pathway (noncanonical).²⁰ While the biological relevance of Wnt and YAP interactions has been demonstrated for PSC selfrenewal and crypt growth in the mouse small intestine, ¹⁹ the biological relevance on neural patterning of hPSCs has not been studied. In addition, stiffening stem cell aggregates with microparticles, which are extensively used for growth factor and drug delivery, ²¹ may affect biophysical microenvironment of the cells. ^{22,23} Incorporation of microparticles also has the potential to overcome the diffusion limitation in large spheroids/organoids.²¹ But the influence of microparticle incorporation on Wnt-YAP interactions has not been investigated. Revealing the convergence of Wnt and YAP during neural tissue patterning from hiPSCs may allow predicting and modulating brain tissue structure and function through the regulation of extracellular microenvironment.

The objective of this study is to investigate the effects of Wnt signaling and YAP expression on the cellular population (i.e., cortical forebrain vs. hindbrain/spinal cord identity) in 3D neural spheroids derived from hiPSCs using Wnt activator CHIR99021 and YAP modulator Cytochalasin D (CytoD). To perturb neural patterning, the corporation of hiPSC-derived neural spheroids with polycaprolactone-poly(dimethylsiloxane)-polycaprolactone (PCL-PDMS-PCL) microparticles was also evaluated. This study should advance our understanding on the patterning of neural tissue with defined structure from hPSCs for future neurological disease modeling, drug screening, and neural tissue regeneration.

Materials and Methods

Undifferentiated human iPSC culture

Human iPSK3 cells were derived from human foreskin fibroblasts transfected with plasmid DNA encoding reprogramming factors OCT4, NANOG, SOX2, and LIN28 (kindly provided by Dr. Stephen Duncan, Medical College of Wisconsin, and Dr. David Gilbert, Department of Biological Sciences of Florida State University). 24,25 Human

iPSK3 cells were maintained in mTeSR serum-free medium (StemCell Technologies, Inc., Vancouver, Canada) on sixwell plates coated with growth factor reduced Geltrex (Life Technologies). The cells were passaged by Accutase dissociation every 5–6 days and seeded at 1×10^6 cells per well of six-well plate in the presence of $10\,\mu M$ Y27632 (Sigma) for the first $24\,h.^{26,27}$

Preparation of PCL-PDMS-PCL microparticles

Macromers of PCL_n-block-PDMS_m-block-PCL_n were synthesized by ring-opening polymerization of ε -caprolactone in the presence of $NH_2 - PDMS_m - NH_2$ and tin catalyst. ^{28–30} The repeat units for PCL (Gelest, Inc., Morrisville, PA) segment length were at n=40. The PDMS (Sigma) segment lengths were at m = 58. The chain propagation between oligomers was achieved by adding hexamethylene diisocyanate (Sigma) as a coupling agent. The synthesized copolymer has elastic modulus of 59 MPa. PCL-PDMS-PCL microparticles were fabricated using a reversed phase precipitation method.³¹ Briefly, the copolymer solution in 1.2-dichloromethane was slowly poured into a 1000-mL big beaker containing 500 mL methanol. Microparticles were formed and precipitated when stirring the solution at 100 rpm. The precipitate was filtered to remove the mixture of 1,2-dichloromethane and methanol. After extensive washing, the final products were dried under vacuum for more than 24 h before the use in cell culture. The formed microparticles have an average size of 50–60 µm in diameter.

Neural differentiation of human iPSCs

Human iPSK3 cells were seeded into Ultra-Low Attachment (ULA) 24-well plates (Corning Incorporated, Corning, NY) at 3×10^5 cells per well in differentiation medium composed of Dulbecco's modified Eagle's medium/Nutrient Mixture F-12 (DMEM/F-12) plus 2% B27 serum-free supplement (Life Technologies). 27,32 For some experiments, iPSK3 cells were seeded in ULA 96-well plates at various numbers (0.65, 1.25, 2.5, and 5×10^4 cells) per well to evaluate the effect of seeding cell number on the aggregate size. Y27632 (10 µM) was added during the seeding and removed after 24 h. At day 1, the cells formed embryoid bodies (EBs) and were treated with dual SMAD signaling inhibitors: 10 µM SB431542 (Sigma) and 100 nM LDN193189 (Sigma) referred to as LDN/SB. After 7 days, the cells were treated with fibroblast growth factor (FGF)-2 (10 ng/mL) and RA (5 μ M; Sigma). 27,32 After another 8 days in suspension, the 3D NPC spheroids (day 16) were replated onto Geltrex-coated surface. For no growth factor protocol, no factor was added during day 0–16. Next day after replating, the cells were treated with Wnt activator CHIR99021 (StemCell Technologies, Inc.) at 10 μM (CHIR+). The cells without the treatment were used as the control (CHIR-). After 5 days of CHIR treatment, the cells were characterized. For CytoD treatment, 2 days after replating, the cells were treated with 1 µM CytoD (Sigma) for 48-72 h before characterization. The cells without the treatment were used as the control.

For neural differentiation based on EB formation with PCL-PDMS-PCL microparticles, PCL-PDMS-PCL microparticles were sterilized with 70% ethanol and then washed three times with phosphate-buffered saline (PBS). The microparticles (0.2 mg/mL) were mixed with the hiPSK3 cells and seeded in low attachment 24-well plates at 3×10^5 cells

per well in differentiation medium and Y27632. The differentiation protocol and all the treatments followed the same procedure to the differentiation without the particles.

Aggregate size distribution

The images of NPC spheroids were captured over the culture time (7 days) by a phase contrast microscopy. The captured images were converted to binary images using ImageJ software (http://rsb.info.nih.gov/ij) and analyzed with the "particle analysis tool." Through particle analysis in ImageJ software, the Feret's diameter of each aggregate in the images can be calculated, which provided the size distribution of the spheroids.³³

Bromodeoxyuridine assay

Briefly, the cells were incubated in growth medium containing $10\,\mu\text{M}$ Bromodeoxyuridine (BrdU) (Sigma) for 90 min. The cells were then fixed with 70% cold ethanol, followed by a denaturation step using 2 N HCl/0.5% Triton X-100 for 30 min in the dark. The samples were reduced with 1 mg/mL sodium borohydride for 5 min and incubated with mouse anti-BrdU (1:100; Life Technologies) in blocking buffer (0.5% Tween 20/1% bovine serum albumin in PBS), followed by the incubation with Alexa Fluor 488 goat anti-Mouse IgG₁ (1:100; Life Technologies). The cells were counterstained with Hoechst 33342 and visualized using a fluorescent microscope (Olympus IX70, Melville, NY).

Immunocytochemistry

Briefly, the samples were fixed with 4% paraformaldehyde (PFA) and permeabilized with 0.2-0.5% Triton X-100 for intracellular markers. The samples were then blocked and incubated with various mouse or rabbit primary antibodies (Supplementary Table S1; Supplementary Data are available online at www.liebertpub.com/tea). After washing, the cells were incubated with the corresponding secondary antibody: Alexa Fluor 488 goat anti-Mouse IgG or Alexa Fluor 594 goat anti-Rabbit IgG (Life Technologies). The samples with second antibody only were used as negative control. For F-actin staining, the cells were incubated with Alexa Fluor 594 Phalloidin (Life Technologies). The samples were counterstained with Hoechst 33342 and visualized using a fluorescent microscope (Olympus IX70, Melville, NY) or a confocal microscope (Zeiss LSM 880). The images (for HOXB4 and TBR1) from five independent fields were analyzed using ImageJ software. The proportion of positive cells was calculated based on the area of marker of interest normalized to the nuclei, indicating the relative expression among different conditions. Nuclear and cytoplasmic YAP was determined based on the expression pattern of image analysis using ImageJ software. The Hoechst expression of each image was superimposed on YAP image. Then, the nuclear YAP was counted and compared with the total Hoechst to obtain the relative expression (Supplementary Fig. S1A).

Flow cytometry

To quantify the levels of various neural marker expressions, the cells were harvested by trypsinization and analyzed by flow cytometry. 34 Briefly, 1×10^6 cells per sample were fixed with 4% PFA and washed with staining buffer (2% fetal bovine serum in PBS). The cells were permeabilized with 100% cold methanol for intracellular markers, blocked, and then incubated with primary antibodies against Nestin, PAX6, β -tubulin III, or MAP-2 followed by the corresponding secondary antibody (Supplementary Table S1). The cells were acquired with BD FACSCantoTM II flow cytometer (Becton Dickinson) and analyzed against isotype controls (negative controls) using FlowJo software.

Reverse transcription polymerase chain reaction analysis

Total RNA was isolated from neural cell samples using the RNeasy Mini Kit (Qiagen, Valencia, CA) according to the manufacturer's protocol followed by the treatment of the DNA-Free RNA Kit (Zymo, Irvine, CA). Reverse transcription was carried out using 2 µg of total RNA, anchored oligo-dT primers (Operon, Huntsville, AL), and Superscript III (Invitrogen, Carlsbad, CA) (according to the protocol of the manufacturer). Primers specific for target genes (Table 1) were designed using the software Oligo Explorer 1.2 (Gene Link, Hawthorne, NY; Table 1). The gene β-actin was used as an endogenous control for normalization of expression levels. Real-time reverse transcription-polymerase chain reaction (RT-PCR) were performed on an ABI7500 instrument (Applied Biosystems, Foster City, CA), using SYBR1 Green PCR Master Mix (Applied Biosystems). The amplification reactions were performed as follows: 2 min at 50°C, 10 min at 95°C, and 40 cycles of 95°C for 15 s and 55°C for 30 s, and 68°C for 30 s. Fold variation in gene expression was quantified by means of the comparative Ct method: $2^{-(C_t t_{reatment} - C_t control)}$, which is based on the comparison of expression of the target gene (normalized to the endogenous control β -actin) between the test samples and the cells from standard differentiation (no particle, no treatment).

Statistical analysis

Each experiment was carried out at least three times. The representative experiments were presented and the results were expressed as (mean \pm standard deviation). To assess the

TABLE 1. PRIMER SEQUENCE FOR TARGET GENES

Gene	Forward primer 5'-3'	Reverse primer 5'–3'
TBR1	CCCCCTCGTCTTTCTCTTACC	TAATGTGGAGGCCGAGACTTG
HOXB4	AATTCCTTCTCCAGCTCCAAGA	CCTGGATGCGCAAAGTTCA
MNX1 (HB9)	GCACCAGTTCAAGCTCAACA	TTTGCTGCGTTTCCATTTC
vGluT1	CCCCAATTCCTCGCACTTTAT	GGGAAGGATCCCAGATTTTGA
Beta-actin	GTACTCCGTGTGGATCGGCG	AAGCATTTGCGGTGGACGATGG

statistical significance, one-way analysis of variance (ANOVA) followed by Fisher's LSD *post hoc* tests were performed. A *p*-value <0.05 was considered statistically significant.

Results

Neural tissue patterning from hiPSCs

Neural tissue patterning in this study was performed using two different protocols: (1) no growth factor protocol for spontaneous neural differentiation (with cell fate of forebrain/midbrain/hindbrain), (2) LDN/SB protocol (dual SMAD inhibition) followed by FGF-2/RA treatment which favors forebrain differentiation (Fig. 1A). In general, undifferentiated hiPSK3 cells formed EBs in low attachment plate for a total of 15–16 days. When replating the formed NPC spheroids, neural cells grew out of the spheres and displayed β-tubulin III expression and Nestin expression (Fig. 1B). Examination of the replated cells showed the cells with

F-actin stress fibers and cells with non-fibrous F-actin expression (Fig. 1C). YAP expression also showed a mixture of cells with nuclear YAP and cells with cytoplasmic YAP (Supplementary Fig. S1B).

The comparison of the no growth factor protocol (–LDN/SB) and the +LDN/SB protocol was performed in low-attachment 96-well plates at a defined seeded cell number (6.5, 12.5, 25, 50K) (Fig. 2). The aggregate size increased with the seeded cell number for both protocols (Fig. 2A, B). In the absence of LDN/SB, the aggregate size was larger than the protocol of +LDN/SB, indicating a selective process for LDN/SB induction. For –LDN/SB condition, TBR1 (a cortical forebrain neural marker) expression was less than +LDN/SB condition, whereas HOXB4 (a hindbrain/spinal cord marker) expression was higher than +LDN/SB protocol (Fig. 2C). TBR1 and HOXB4 were expressed on the side region of the aggregates, showing the polarity of the NPC spheroids (Fig. 2D). These results indicate that LDN/SB

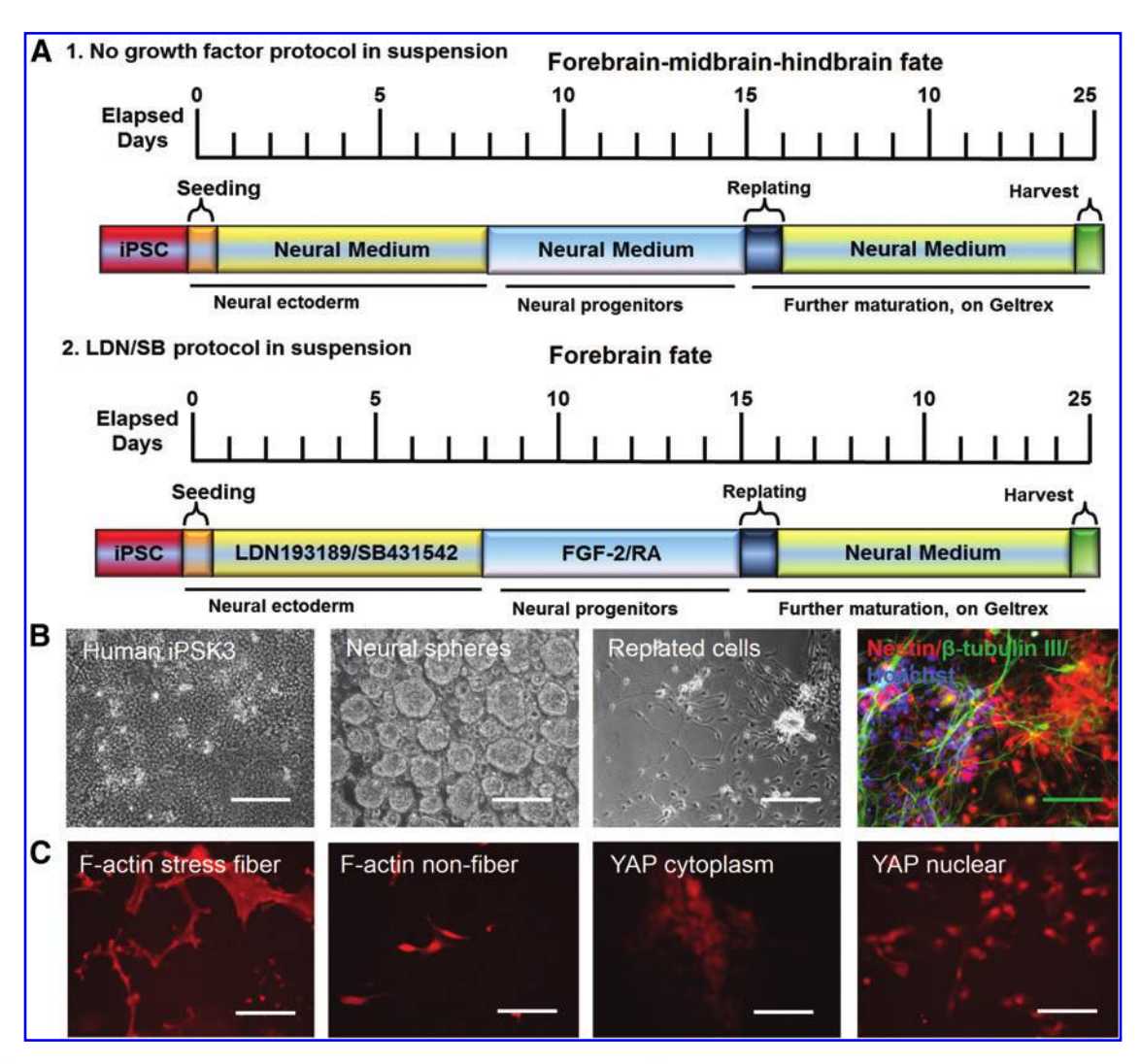


FIG. 1. Procedures of neural lineage commitment from hiPSCs. (A) Illustration of the neural induction protocols from hiPSCs. (B) Representative morphology of human iSK3 cells along neural differentiation and the representative neural marker expression. Scale bar (*white*): 200 μm. Scale bar (*green*): 100 μm. (C) Representative expression of YAP and F-actin for the differentiated cells. Scale bar: 50 μm. The cells displayed both F-actin stress fibers and the nonfiber F-actin. Some cells have nuclear YAP expression and some cells have cytoplasmic YAP expression. hiPSC, human induced pluripotent stem cell; YAP, Yes-associated protein. Color images available online at www.liebertpub.com/tea

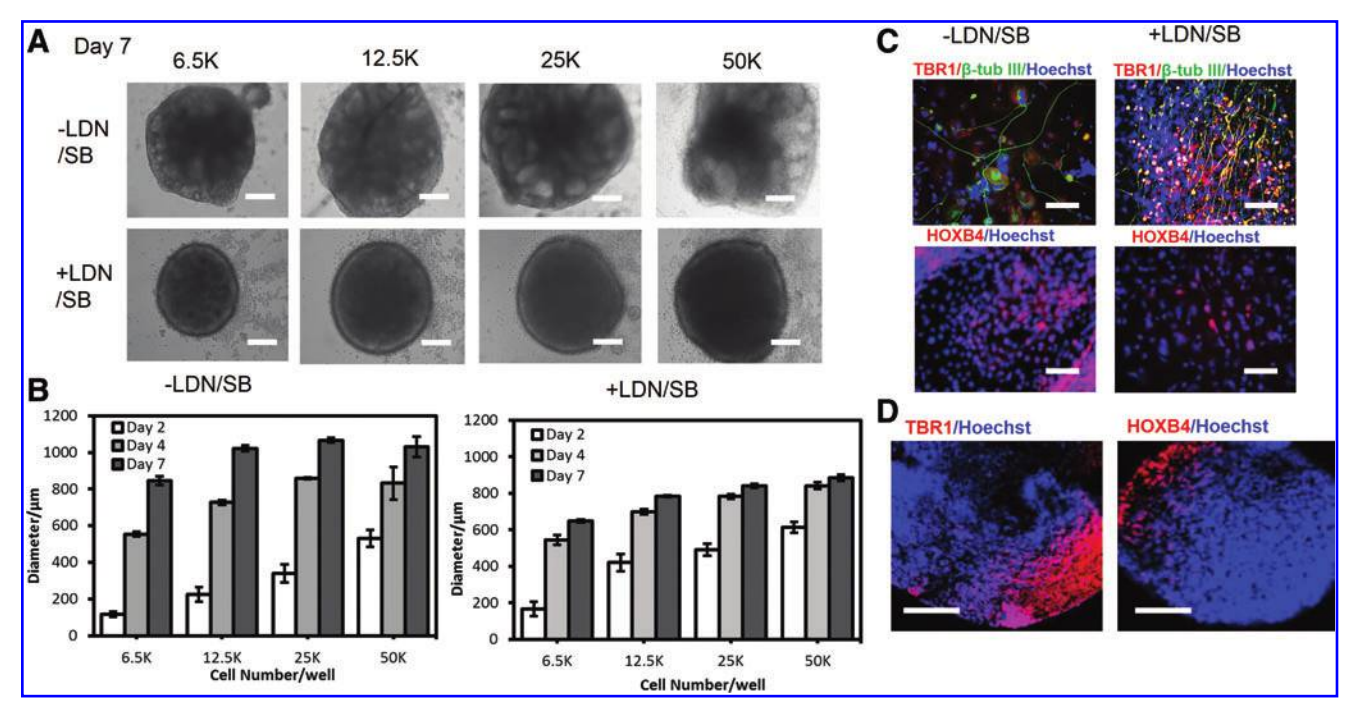


FIG. 2. Comparison of neural progenitor spheroid formation from hiPSCs with no factors versus LDN/SB induction. The comparison was performed in a low attachment 96-well plate. Each well was seeded with different numbers (0.65e4, 1.25e4, 2.5 e4, and 5e4) of hiPSK3 cells in DMEM/F-12 plus B27 medium. (**A**) Day 7 morphology of NPC aggregates with no factors versus LDN/SB induction. Scale bar: 200 μm. (**B**) The average aggregate size at day 2, 4, and 7 for the two types of induction methods. (**C**) The expression of TBR1, HOXB4, and β-tubulin III of the replated cells at day 14 for the two types of neural ectoderm induction. Scale bar: 100 μm. (**D**) Confocal images of NPC spheroids (day 16) using LDN/SB induction to reveal the localization of TBR1 and HOXB4. Scale bar: 200 μm. NPC, neural progenitor cell. Color images available online at www.liebertpub.com/tea

induction influence neural tissue patterning from hiPSCs and favors cortical forebrain cells.

Effect of CHIR on neural tissue patterning from hiPSCs

To further elucidate the influence of Wnt activation on neural tissue patterning of hiPSCs, the CHIR-treated cells were evaluated for neural differentiation and TBR1 and HOXB4 expression. To create biophysical perturbation and demonstrate the feasibility of using microparticles in hiPSC spheroid culture, PCL-PDMS-PCL microparticles were incorporated during EB formation (with particle) in comparison to the condition without microparticles (no particle). First, the neural differentiation was induced in the absence of LDN/SB and other growth factors (Fig. 3). The morphology of the NPC spheres and the replated cells was shown in Figure 3A. The day 15+5 cells expressed Nestin but few β-tubulin III (data not shown). The presence of CHIR reduced Nestin expression (from 80.3% to 60.5%), probably due to the proliferation of non-neuronal cells (Fig. 3B). The "with particle" groups followed a similar trend (Nestin expression was 97.6% vs. 28.8% for no treatment vs. CHIR treatment). For neural patterning markers, HOXB4 expression increased $(0.32\pm0.09 \text{ vs. } 0.56\pm0.09)$, whereas TBR1 expression decreased $(0.75 \pm 0.12 \text{ vs. } 0.42 \pm 0.05)$ with CHIR treatment compared with no CHIR treatment (Fig. 3C, D). Again, the with particle groups showed a similar trend, but the difference was not statistically significant.

Similar experiments were performed for LDN/SB-induced neural differentiation (Fig. 4). The presence of CHIR reduced Nestin expression (from 61.6% to 34.4%) and slightly increased β-tubulin III (from 58.9% to 67.6%) (Fig. 4A). MAP-2 expression was increased by CHIR treatment for no particle groups, but not for with particle groups (Supplementary Fig. S2). For neural patterning markers, while HOXB4 expression increased with CHIR treatment, the increase was not statistically significant (Fig. 4B, C). TBR1 expression significantly decreased with CHIR treatment (from 0.35 ± 0.02 to 0.17 ± 0.02 for no particle groups, from 0.45 ± 0.03 to 0.30 ± 0.05 for with particle groups). To further identify the effect of CHIR treatment, RT-PCR analysis was performed for the gene expression of HOXB4, TBR1, and HB9 (Fig. 5A). HOXB4 gene expression increased with CHIR treatment (from 0.96 ± 0.02 to 1.34 ± 0.12) and TBR1 expression decreased (from 0.99 ± 0.02 to 0.47 ± 0.22) with CHIR treatment for no particle groups. With particles, similar trend was observed. No significant changes were observed for HB9 expression after CHIR treatment, may be due to the immature stage of caudal cell population. To further confirm the influence of CHIR treatment on neural patterning, additional markers for forebrain identity (PAX6 and BRN2) and hindbrain/motor neuron identity (Islet-1; ISL1) were evaluated (Fig. 5B and Supplementary Fig. S3). ISL1 expression was higher, whereas PAX6 and BRN2 expression was lower after CHIR treatment. For all four groups, the neural cells (at day 28) displayed synaptic activity by expressing presynaptic marker Synapsin I and postsynaptic marker PSD95 (Supplementary Fig. S4). These results indicate

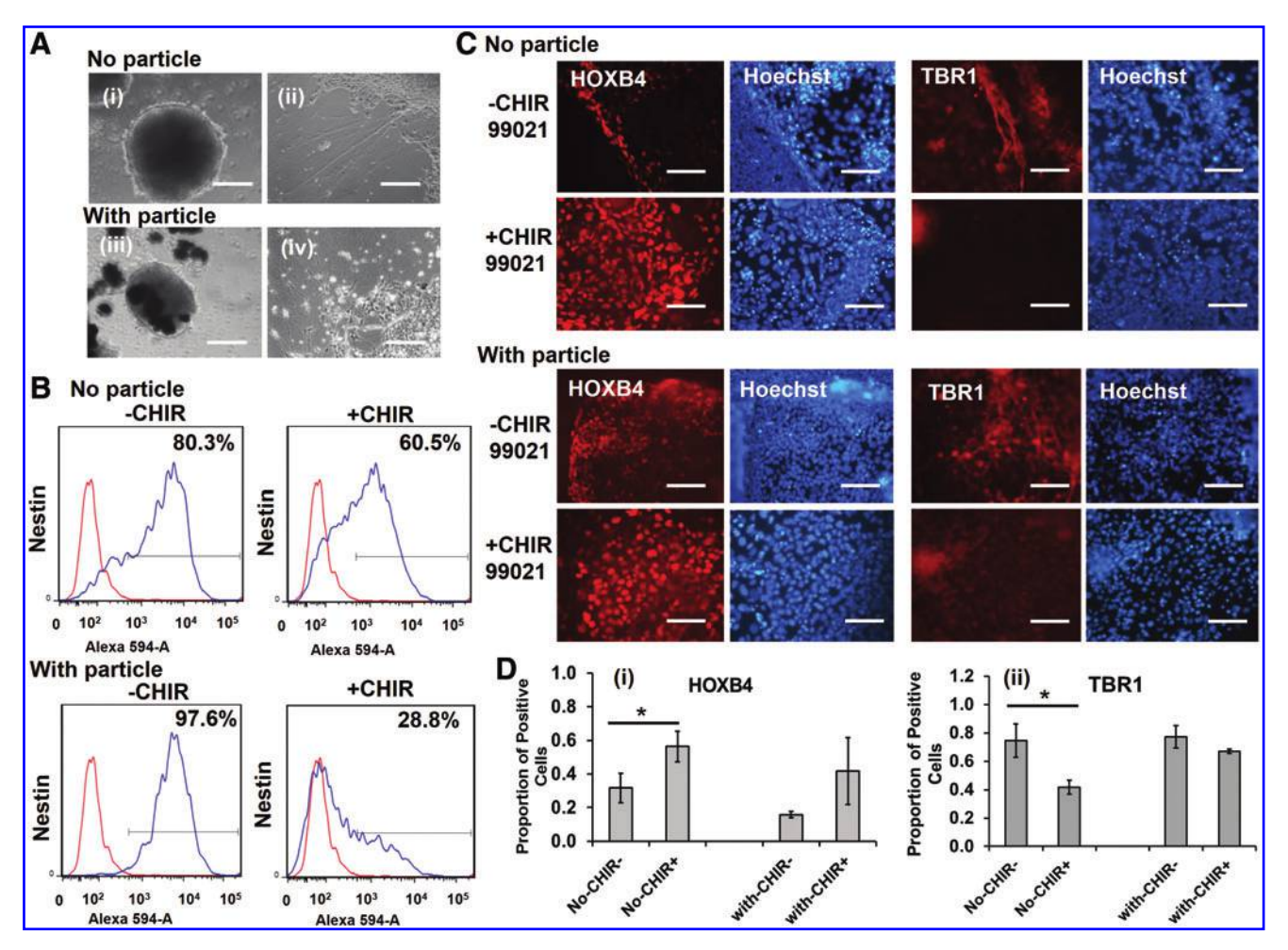


FIG. 3. Effect of CHIR99021 on neural tissue patterning-no growth factor induction. (**A**) Phase contrast images of day 16 NPC spheroids and the replated cells (4 days later). No particle group: (i) floating NPC spheroids; (ii) replated cell outgrowth; with particle group: (iii) floating NPC spheroids; and (iv) replated cell outgrowth. Scale bar: 200 μm. (**B**) Flow cytometry analysis of Nestin expression with ±CHIR 99021 treatment (day 23). The negative control is shown in *red*. (**C**) Fluorescent images of HOXB4 expression and TBR1 expression (day 22) with ±CHIR 99021 treatment. Scale bar: 100 μm. (**D**) Quantification of HOXB4 and TBR1 expression with ±CHIR 99021 treatment. (i) HOXB4, (ii) TBR1. "No" indicates no particle conditions; "With" indicates with particle conditions. **p*-value <0.05. Color images available online at www.liebertpub.com/tea

that Wnt activation by CHIR promotes caudal hindbrain/spinal cord identity and reduces rostral forebrain identity.

Effect of CHIR on YAP expression

The influence of Wnt activator CHIR99021 (CHIR) on YAP expression was then evaluated (Fig. 6A). The day 16 NPC spheroids (LDN/SB induction) were replated and treated with CHIR for 5 days. More nuclear YAP expression (47.8% \pm 9.9% vs. 26.0% \pm 1.3%) was observed after CHIR treatment (p = 0.036) (Fig. 6B, C). The cells with CHIR treatment (more nuclear YAP expression) showed higher proliferation rate and more BrdU⁺ cells (45.3% \pm 2.8% vs. 34.2% \pm 1.2%, Supple-

mentary Fig. S5). Similar trend was observed for the conditions incorporated with microparticles, although some variations existed (nuclear YAP was $52.6\% \pm 3.3\%$ vs. $26.5\% \pm 7.3\%$ for CHIR treatment vs. no treatment, p = 0.005). The replated cells expressed β -tubulin III, indicating the differentiation into neuronal cells. These results indicate that Wnt activation results in nuclear YAP localization.

Effect of CytoD on neural tissue patterning from hiPSCs

To investigate if YAP expression plays a role in Wntregulated neural patterning, ¹⁹ the modulator for YAP expression

FIG. 5. Additional characterizations of neural tissue patterning with LDN/SB induction. (**A**) RT-PCR analysis of HOXB4, HB9 (i), and TBR1 (ii) gene expression (day 21) with ±CHIR 99021 treatment. "No" indicates no particle conditions; "P" indicates with particle conditions. (**B**) Additional neural patterning markers. (i) Islet-1 (ISL1) (*red*)/β-tubulin III (*green*)/Hoechst (*blue*) expression. (ii) PAX6 (*green*)/Hoechst (*blue*) expression, and BRN2 (*red*)/Hoechst (*blue*) expression. Scale bar: 100 μm. **p*-value <0.05. Color images available online at www.liebertpub.com/tea

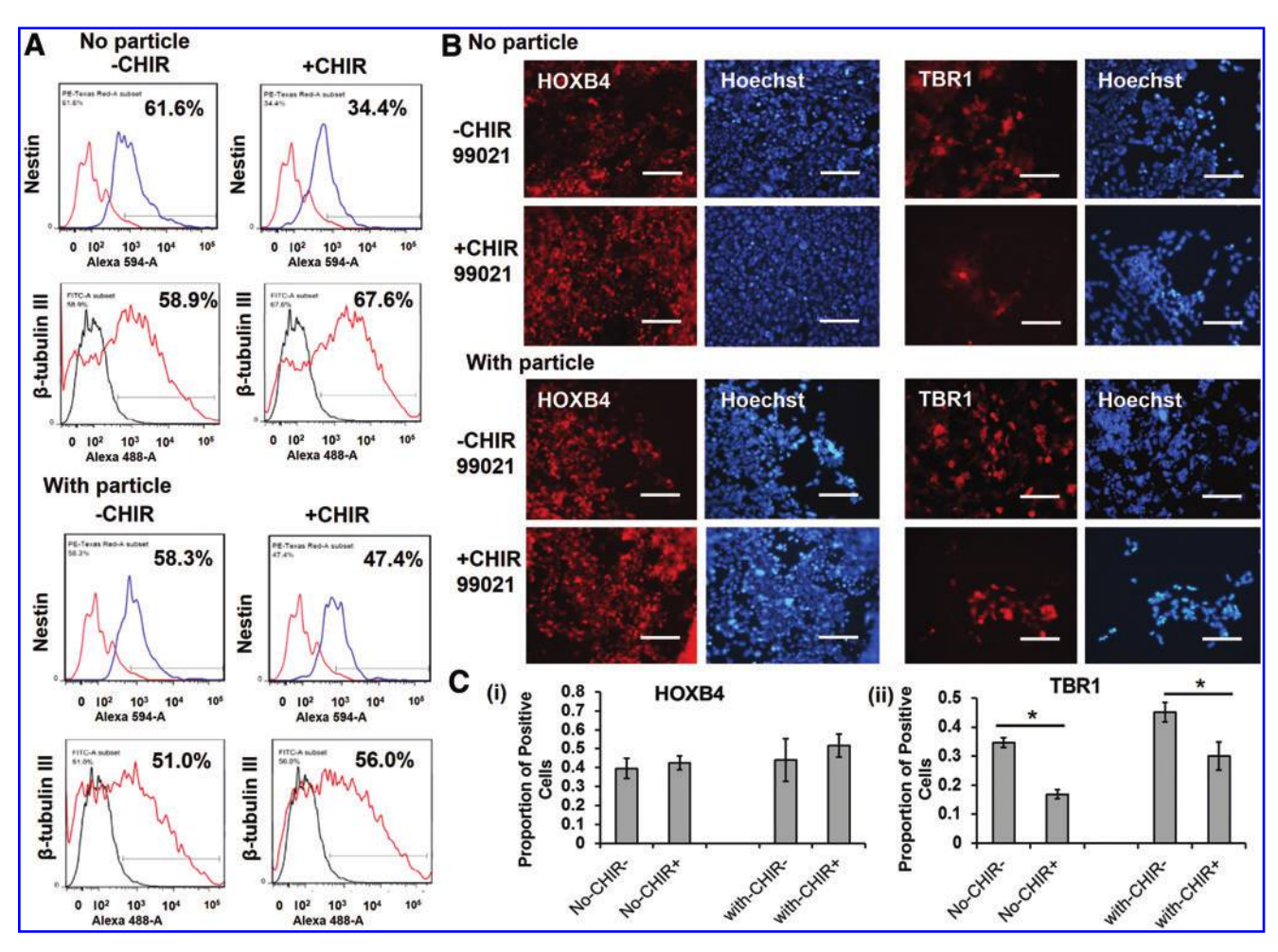
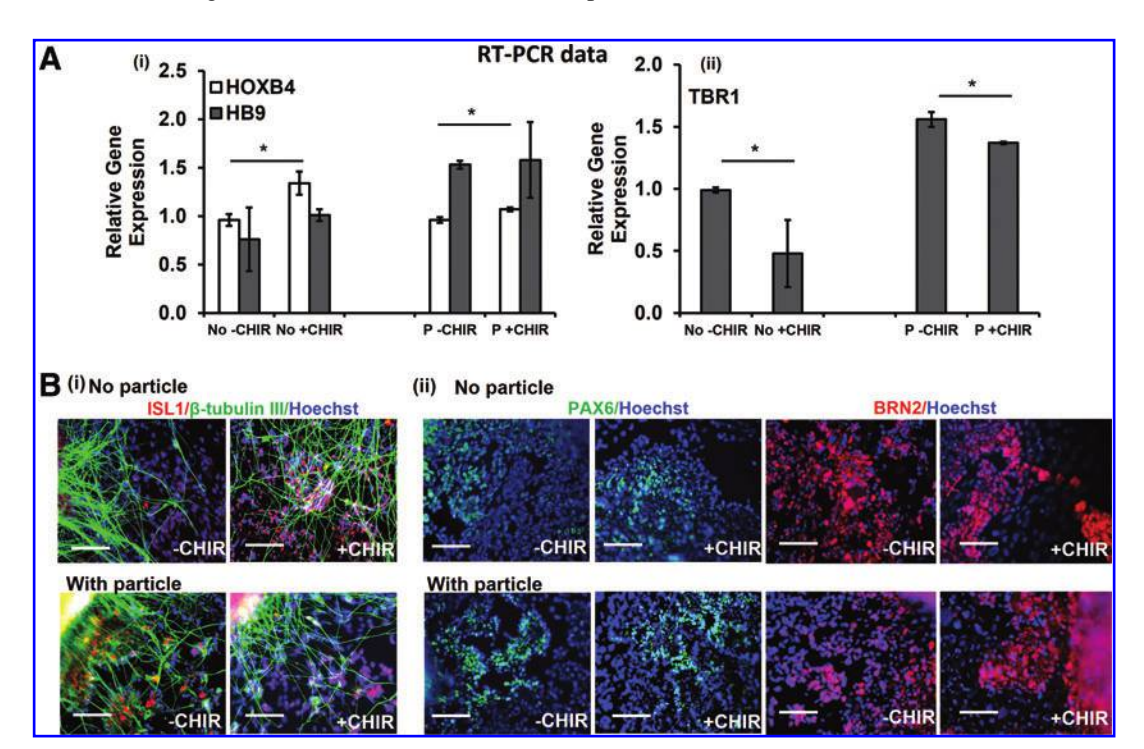


FIG. 4. Effect of CHIR99021 on neural tissue patterning-LDN/SB induction. (**A**) Flow cytometry analysis of Nestin and β-tubulin III expression with ±CHIR 99021 treatment (day 24). For Nestin, the negative control is shown in *red*; for β-tubulin III, the negative control is shown in *black*. (**B**) Fluorescent images of HOXB4 expression and TBR1 expression (day 24) with ±CHIR 99021 treatment. Scale bar: 100 μm. (**C**) Quantification of HOXB4 and TBR1 expression with ±CHIR 99021 treatment. (i) HOXB4, (ii) TBR1. "No" indicates no particle conditions; "With" indicates with particle conditions. **p*-value <0.05. Color images available online at www.liebertpub.com/tea



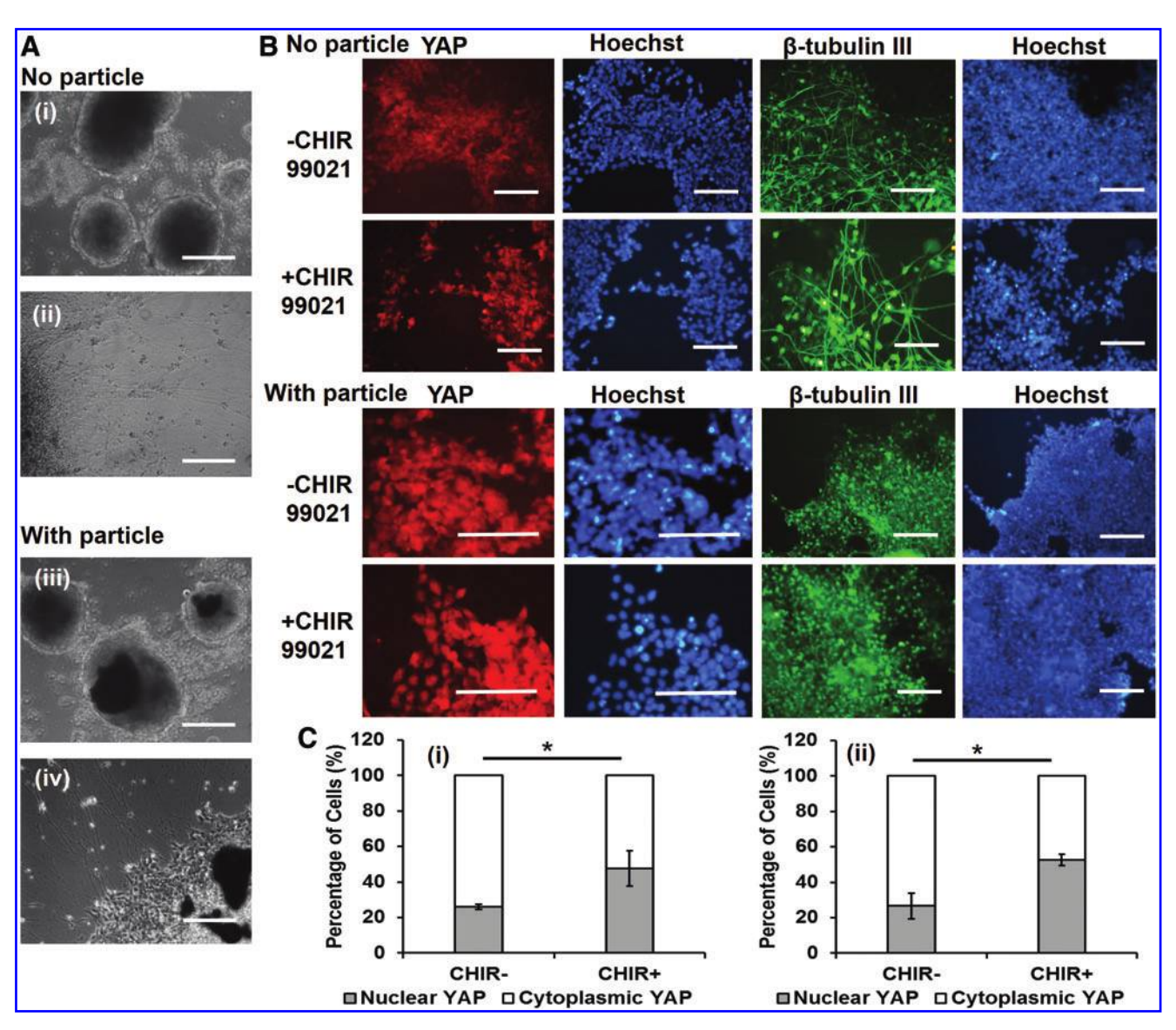


FIG. 6. Effect of CHIR99021 on YAP expression and neural differentiation. (A) Phase contrast images of day 16 NPC spheroids (with LDN/SB induction) and the replated cells (4 days later). No particle group: (i) floating NPC spheroids; (ii) replated cell outgrowth; with particle group: (iii) floating NPC spheroids; and (iv) replated cell outgrowth. Scale bar: $200 \,\mu\text{m}$. (B) Fluorescent images of YAP expression and β-tubulin III expression (day 22) with ±CHIR 99021 treatment. Scale bar: $100 \,\mu\text{m}$. (C) Quantification of cytoplasmic YAP and nuclear YAP expression with ±CHIR 99021 treatment. (i) No particle; (ii) with particle. *p-value <0.05. Color images available online at www.liebertpub.com/tea

was evaluated. CytoD is the actomyosin cytoskeletal molecule that disrupts F-actin and then inhibits YAP nuclear localization. This study, the addition of CytoD was found to induce more neurite outgrowth and cytoplasmic YAP expression (Fig. 7A, B and Supplementary Fig. S6A). Correspondingly, β -catenin expression was more cytoplasmic and higher β -tubulin III expression was observed after addition of CytoD (Fig. 7C and Supplementary Figs. S6B, S7, and S8A). For comparison, treatment with CHIR showed more nuclear expression of β -catenin (Fig. 7C and Supplementary Fig. S7). With the inclusion of microparticles, the trend of CytoD treatment was similar. The influence of CytoD on neural patterning markers TBR1 and HOXB4 was then evaluated (Fig. 8A). The CytoD treatment reduced the expression of HOXB4 protein (from 0.79 \pm 0.12 to 0.29 \pm 0.15) significantly

for no particle groups. The increase in the expression of TBR1 protein was not statistically significant. Similar trends were observed for with particle groups, but the differences were not statistically significant (Fig. 8B). RT-PCR analysis showed the significant decrease of HOXB4 and HB9 expression after CytoD treatment as well as the increase in gene expression of vGlut1, another marker for forebrain cortical cells (Fig. 8C). The increase in TBR1 was statistically insignificant. Analysis of additional markers showed that the glutamate expression was increased and the GABA expression was decreased after CytoD treatment (Supplementary Fig. S8B). These data indicate that YAP modulator CytoD affects neural tissue patterning (decrease caudal identity) and the influence of Wnt and YAP is bidirectional.

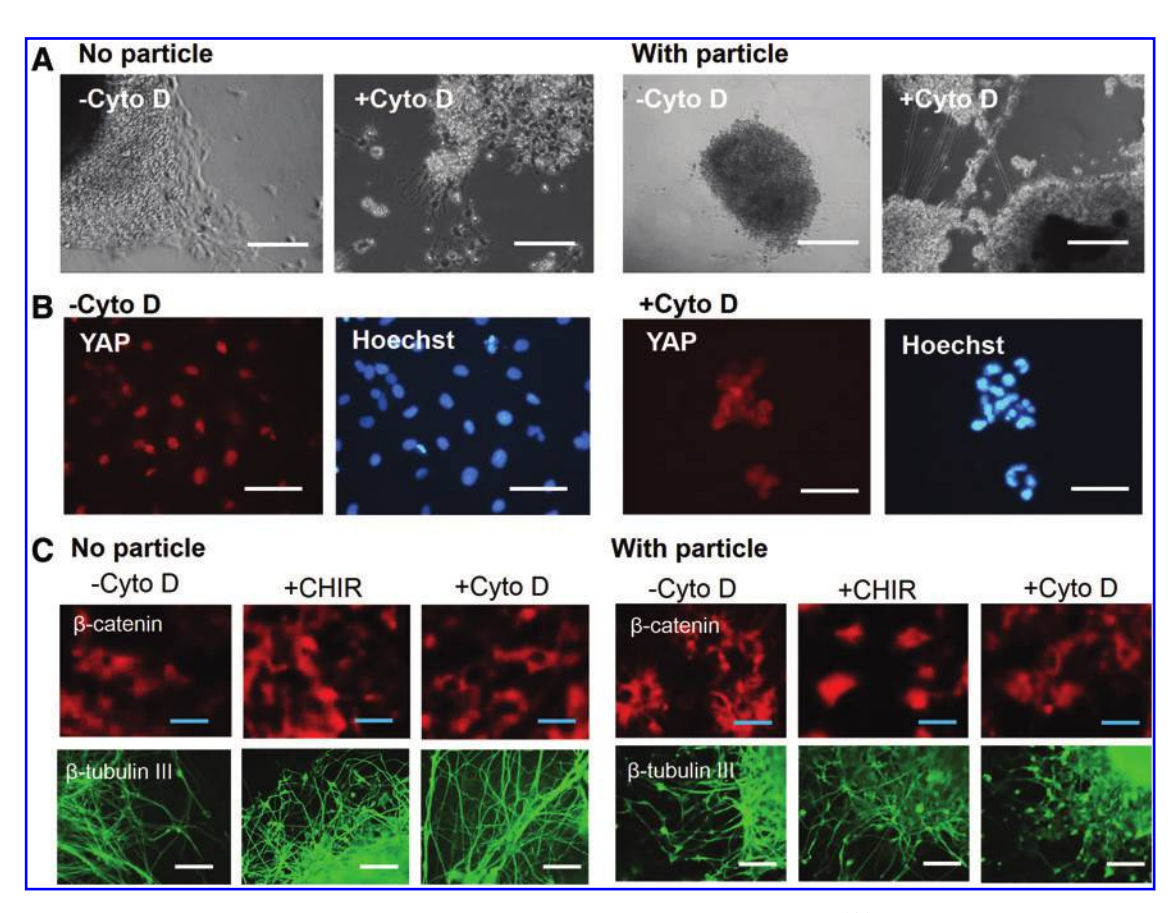


FIG. 7. Effect of CytoD treatment on YAP expression and neural differentiation. (**A**) Phase contrast images of replated NPC spheroids treated with CytoD. Scale bar: $200 \,\mu\text{m}$. (**B**) YAP expression in the outgrowth of the replated NPC spheroids treated with CytoD. Scale bar: $50 \,\mu\text{m}$. (**C**) β-catenin and β-tubulin III expression in the outgrowth of the replated NPC spheroids treated with CytoD. The treatment with CHIR was included for comparison. Scale bar: $100 \,\mu\text{m}$ for β-tubulin III, and $25 \,\mu\text{m}$ for β-catenin. CytoD, cytochalasin D. Color images available online at www.liebertpub.com/tea

Discussion

Wnt signaling plays an important role in patterning neural tissues from hPSCs and has been found to enrich motor neurons or hind brain/spinal cord NPCs. 15,36,37 In the meanwhile, the interaction of Wnt pathway with YAP expression is a critical signaling event during tissue morphogenesis. 19,20 However, the biological relevance of Wnt-YAP interactions in neural patterning of hPSCs has not been well studied, as stated in our previous perspective article. 38 In addition, the influence of biophysical perturbation with microparticles in hPSC-derived neural spheroids has not been well explored. Following our perspective article, 38 the experimental evidence of Wnt signaling and YAP activity in hPSC-derived neural spheroids was revealed in this study.

The role of Wnt signaling in neural tissue patterning

Wnt signaling can be modulated to generate neural cells or tissues of forebrain (Wnt low), midbrain (Wnt medium), or hindbrain (Wnt high) regional specificity together with other signaling pathways such as RA, FGF-2, and Sonic Hedgehog (SHH). While the Wnt-regulated cell proliferation is recognized to be a pivotal regulator in organ growth and tissue regeneration, the detailed mechanism and the

crosstalk with other signaling pathways such as Hippo/YAP have not been well understood in neural patterning of hPSCs.

Our results showed the influence of Wnt regulation (canonical) on YAP expression in the context of neural patterning of hiPSCs into brain-like tissues. CHIR treatment induces nuclear YAP expression and promotes the expression of HOXB4 (a hindbrain/spinal cord marker).⁴⁰ On the contrast, the absence of CHIR treatment and more cytoplasmic YAP expression promotes the expression of TBR1 (a cortical forebrain marker).³⁹ In particular, our results demonstrate the effect of Wnt-mediated neural tissue patterning of hPSCs in a 3D culture. It was recently found that Wnt activation (canonical) results in nuclear YAP localization in HEK293 cells and mouse embryonic stem cells. 19 In the absence of Wnt signaling, YAP/TAZ is relocalized in the cytoplasm by forming the destruction complex. Wnt activation by Wnt 3a shows the possible mechanism of YAP relocalization: the progressive dissociation of YAP/TAZ from Axin and the increased association of Axin to LRP6, release YAP/TAZ from the destruction complex to allow its nuclear localization and the following transcription. 19 An "alternative Wnt-YAP/ TAZ signaling axis" mechanism (noncanonical) was also proposed recently, which is independent of β-catenin activity. 20 Along with these findings in crosstalk of Wnt and

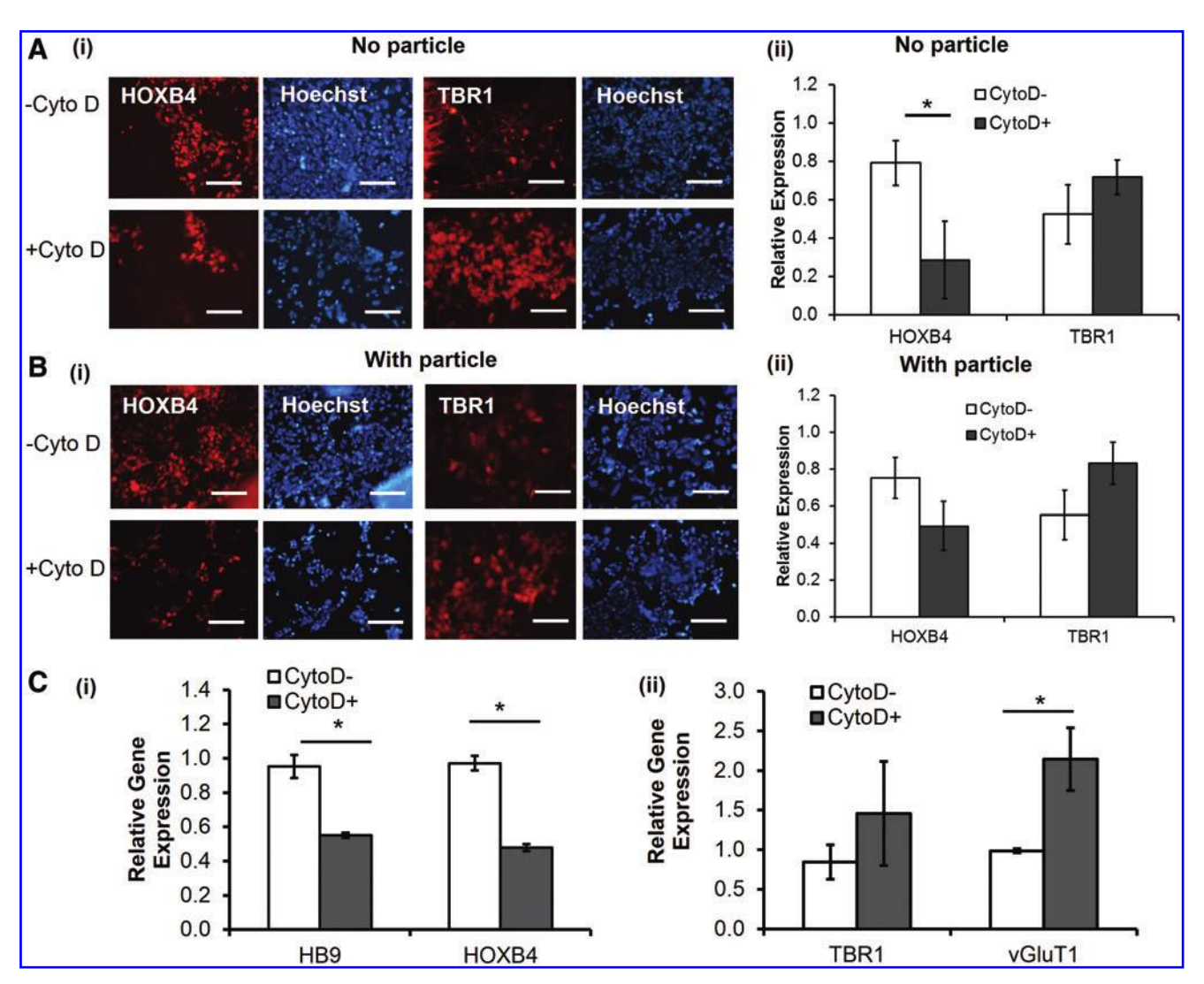


FIG. 8. Effect of CytoD treatment on neural tissue patterning of hiPSCs. (**A**) No particle groups. (i) Fluorescent images of HOXB4 expression and TBR1 expression (day 20) with ±CytoD treatment. Scale bar: 100 μm. (ii) Quantification of HOXB4 expression and TBR1 expression. (**B**) With particle groups. (i) Fluorescent images of HOXB4 expression and TBR1 expression (day 20) with ±CytoD treatment. Scale bar: 100 μm. (ii) Quantification of HOXB4 expression and TBR1 expression. (**C**) (i) RT-PCR analysis of HOXB4 and HB9 expression with ±CytoD treatment (day 20); (ii) RT-PCR analysis of TBR1 and vGlut1 expression with ±CytoD treatment (day 20). *p-value <0.05. Color images available online at www.liebertpub.com/tea

YAP, our study showed the possible Wnt (canonical)/YAP interaction in neural patterning of hiPSCs.

YAP perturbation in neural tissue patterning

YAP expression has been investigated recently as the mediator of mechanotransduction during stem cell differentiation. The intracellular mechanical rheostat that controls mechanical memory behavior of stem cells, and the regulator of organ size control. And In terms of neural differentiation from hiPSCs, nuclear YAP localization may need to be inhibited. For example, inhibition of Hippo/YAP signaling on soft surface, which results in cytoplasmic YAP expression, promoted motor neuron differentiation from hiPSCs in the presence of soluble neurogenic factors. In the absence of neurogenic factors, GABAergic neurons were enriched during neuronal differentiation of hPSCs on soft substrate that inhibited nuclear localization of YAP.

actions of YAP expression and canonical Wnt activity in neural patterning of hiPSCs remains unexplored.

As we stated previously, ³⁸ Hippo/YAP pathway may regulate YAP/TAZ localization and activate or inhibit Wnt signaling in two ways. ⁴⁷ (a) In cell nuclei, inhibition of Hippo pathway activates YAP as well as β -catenin-regulated genes (i.e., nuclear YAP promotes Wnt). YAP and β -catenin can form YAP- β -catenin complex to stabilize nuclear expression. (b) In cell cytoplasm, cytoplasmic YAP (i.e., activation of Hippo) can sequester β -catenin in cytoplasm (i.e., cytoplasmic YAP inhibits Wnt). Therefore, the retention of cytoplasmic β -catenin is promoted and Wnt signaling is inhibited. While Wnt activation results in nuclear localization of YAP, YAP localization may also influence Wnt pathway, indicating bidirectional interactions.

Given the possible interactions between Wnt pathway and YAP expression,¹⁷ we hypothesize that the perturbation of YAP protein localization affects Wnt pathway and

neural tissue patterning from hiPSCs. 38 To prove this experimentally, in this study, we used CytoD, an actomyosin cytoskeletal molecule that disrupts F-actin stress fibers, to inhibit YAP nuclear localization. 35 Stress fibers can reduce YAP phosphorylation and promote nuclear YAP, 48 and the mechanotransduction role of YAP is also related to the Rho GTPase signaling through cytoskeleton polymerization. 49 Our results indicated that CytoD treatment induces cytoplasmic expression of β -catenin and influences the patterning of neural tissues from hiPSCs (i.e., decreasing HOXB4 expression), acting as a modulator such as Wnt inhibitors.

The Wnt/YAP interactions have been revealed recently to be β -catenin dependent (canonical) or β -catenin independent (noncanonical). It is thought that the biological context of studying Wnt/YAP interactions and the influence of additional pathways may be critical. Our results here are more supportive of β -catenin-dependent (canonical Wnt pathway) mechanism in the context of neural patterning of hiPSCs. Nonetheless, the complex signaling networks in the stem cells are far from a complete understanding to date and need further systematic explorations.

The influence of microparticles

Biophysical perturbation of neural spheroids derived from hiPSCs by incorporating PCL-PDMS-PCL microparticles may influence neural tissue patterning of hiPSCs. Microparticles have been commonly used for drug/growth factor delivery as well as substrates for tissue engineering. 21,23,50 The biochemical motifs of microparticles showed significant effects on the localized and on-site stem cell differentiation. 21,51,52 The presence of microparticles may alter extracellular matrix remodeling by influencing the matrix metalloproteinase activity. 53 Therefore, this study investigates the influence of biophysical perturbation caused by microparticles in the context of 3D neural patterning of hiPSCs.

Our results indicated that the presence of PCL-PDMS-PCL microparticles maintained similar trends to the groups in the absence of microparticles for cell response to the CHIR or CytoD treatment, while some variations were observed. The influence of microparticles is affected by various parameters such as materials chemistry, particle size, particle stiffness, and the amount of particles that are incorporated into the spheroids, which may contribute to the variations. 21,51,52 In addition, the interactions of microparticles with the cells in the stem cell aggregates, where cell-cell interactions may dominate cell-matrix interactions, are different from the cellparticle interactions for the cells adhered on two-dimensional substrates. However, our results reveal the extent to which the microparticles affect neural patterning of hiPSCs along with the Wnt/YAP interactions. The potential use of microparticles for biomolecule delivery inside neural spheroids as seen in the applications of brain organoid derivation from hPSCs⁶ may require the rational design of microparticle properties such as appropriate size and stiffness (e.g., similar to elastic modulus of stem cell aggregates).

Self-organization of hiPSCs into neural tissues or miniorgan like structures is affected by a signaling network that involves biochemical and biophysical extracellular signals as well as the crosstalk of a series of intracellular signaling pathways. ^{2,10,54,55} By understanding the influence of Wnt and YAP

on neural tissue patterning from hiPSCs, the gained knowledge should advance our long-term objective to allow predicting and modulating brain-like tissue structure and function through the regulation of extracellular microenvironment.

Conclusions

This study indicates that Wnt activation induces nuclear YAP localization and the caudalization of neural cells, and affects neural tissue patterning from hiPSCs by modulating rostral and caudal brain tissue identity. On the other hand, modulating YAP expression by CytoD affects β -catenin expression and thus neural tissue patterning from hiPSCs. Biophysical perturbation of NPC spheroid formation by PCL-PDMS-PCL microparticles maintains similar trends of the cell responses to the CHIR or CytoD treatment. This study provides new insights of Wnt/YAP interactions in the context of neural tissue patterning from hiPSCs and has significance in 3D neural tissue modeling and brain organoid generation.

Acknowledgments

The authors would like to thank Ms. Ruth Didier in FSU Department of Biomedical Sciences for her help with flow cytometry analysis, Dr. Brian K. Washburn and Kristina Poduch in FSU Department of Biological Sciences for their help with RT-PCR analysis, Dr. Stephen Duncan at Medical College of Wisconsin and Dr. David Gilbert in FSU Department of Biological Sciences for human iPSK3 cells, and Mr. Peter Sahwell for his help on image analysis. This work is supported by FSU start up fund, FSU COFRS award, FSU Bridge Grant, National Science Foundation (grant nos. 1342192 and 1652992 to Y.L.). Research reported in this publication was supported by the National Institute of Biomedical Imaging and Bioengineering of the National Institutes of Health under Award Number R03EB020770 (to Y.L.). The content is solely the responsibility of the authors and does not necessarily represent the official views of the National Institutes of Health.

Disclosure Statement

No competing financial interests exist.

References

- Lancaster, M.A., Renner, M., Martin, C.A., Wenzel, D., Bicknell, L.S., Hurles, M.E., Homfray, T., Penninger, J.M., Jackson, A.P., and Knoblich, J.A. Cerebral organoids model human brain development and microcephaly. <u>Nature</u> 501, 373, 2013.
- Lancaster, M.A., and Knoblich, J.A. Organogenesis in a dish: modeling development and disease using organoid technologies. Science 345, 1247125, 2014.
- Pasca, A.M., Sloan, S.A., Clarke, L.E., Tian, Y., Makinson, C.D., Huber, N., Kim, C.H., Park, J.Y., O'Rourke, N.A., Nguyen, K.D., Smith, S.J., Huguenard, J.R., Geschwind, D.H., Barres, B.A., and Pasca, S.P. Functional cortical neurons and astrocytes from human pluripotent stem cells in 3D culture. Nat Methods 12, 671, 2015.
- Yin, X., Mead, B.E., Safaee, H., Langer, R., Karp, J.M., and Levy, O. Engineering stem cell organoids. <u>Cell Stem</u> Cell 18, 25, 2016.

- Jo, J., Xiao, Y., Sun, A.X., Cukuroglu, E., Tran, H.D., Goke, J., Tan, Z.Y., Saw, T.Y., Tan, C.P., Lokman, H., Lee, Y., Kim, D., Ko, H.S., Kim, S.O., Park, J.H., Cho, N.J., Hyde, T.M., Kleinman, J.E., Shin, J.H., Weinberger, D.R., Tan, E.K., Je, H.S., and Ng, H.H. Midbrain-like organoids from human pluripotent stem cells contain functional dopaminergic and neuromelanin-producing neurons. <u>Cell</u> Stem Cell 19, 248, 2016.
- Qian, X., Nguyen, H.N., Song, M.M., Hadiono, C., Ogden, S.C., Hammack, C., Yao, B., Hamersky, G.R., Jacob, F., Zhong, C., Yoon, K.J., Jeang, W., Lin, L., Li, Y., Thakor, J., Berg, D.A., Zhang, C., Kang, E., Chickering, M., Nauen, D., Ho, C.Y., Wen, Z., Christian, K.M., Shi, P.Y., Maher, B.J., Wu, H., Jin, P., Tang, H., Song, H., and Ming, G.L. Brain-region-specific organoids using mini-bioreactors for modeling ZIKV exposure. Cell 165, 1238, 2016.
- Israel, M.A., Yuan, S.H., Bardy, C., Reyna, S.M., Mu, Y., Herrera, C., Hefferan, M.P., Van Gorp, S., Nazor, K.L., Boscolo, F.S., Carson, C.T., Laurent, L.C., Marsala, M., Gage, F.H., Remes, A.M., Koo, E.H., and Goldstein, L.S. Probing sporadic and familial Alzheimer's disease using induced pluripotent stem cells. Nature 482, 216, 2012.
- 8. Dimos, J.T., Rodolfa, K.T., Niakan, K.K., Weisenthal, L.M., Mitsumoto, H., Chung, W., Croft, G.F., Saphier, G., Leibel, R., Goland, R., Wichterle, H., Henderson, C.E., and Eggan, K. Induced pluripotent stem cells generated from patients with ALS can be differentiated into motor neurons. Science 321, 1218, 2008.
- Schwartz, M.P., Hou, Z., Propson, N.E., Zhang, J., Engstrom, C.J., Costa, V.S., Jiang, P., Nguyen, B.K., Bolin, J.M., Daly, W., Wang, Y., Stewart, R., Page, C.D., Murphy, W.L., and Thomson, J.A. Human pluripotent stem cell-derived neural constructs for predicting neural toxicity. Proc Natl Acad Sci U S A 112, 12516, 2015.
- 10. Li, Y., Xu, C., and Ma, T. In vitro organogenesis from pluripotent stem cells. Organogenesis 10, 159, 2014.
- 11. Blauwkamp, T.A., Nigam, S., Ardehali, R., Weissman, I.L., and Nusse, R. Endogenous Wnt signalling in human embryonic stem cells generates an equilibrium of distinct lineage-specified progenitors. Nat Commun 3, 1070, 2012.
- MacDonald, B.T., Tamai, K., and He, X. Wnt/beta-catenin signaling: components, mechanisms, and diseases. <u>Dev</u> Cell 17, 9, 2009.
- 13. Azarin, S.M., Lian, X., Larson, E.A., Popelka, H.M., de Pablo, J.J., and Palecek, S.P. Modulation of Wnt/beta-catenin signaling in human embryonic stem cells using a 3-D microwell array. Biomaterials **33**, 2041, 2012.
- 14. Maury, Y., Come, J., Piskorowski, R.A., Salah-Mohellibi, N., Chevaleyre, V., Peschanski, M., Martinat, C., and Nedelec, S. Combinatorial analysis of developmental cues efficiently converts human pluripotent stem cells into multiple neuronal subtypes. Nat Biotechnol 33, 89, 2015.
- Moya, N., Cutts, J., Gaasterland, T., Willert, K., and Brafman, D.A. Endogenous WNT signaling regulates hPSC-derived neural progenitor cell heterogeneity and specifies their regional identity. <u>Stem Cell Reports</u> 3, 1015, 2014.
- Du, Z.W., Chen, H., Liu, H., Lu, J., Qian, K., Huang, C.L., Zhong, X., Fan, F., and Zhang, S.C. Generation and expansion of highly pure motor neuron progenitors from human pluripotent stem cells. Nat Commun 6, 6626, 2015.
- Konsavage, W.M., Jr., and Yochum, G.S. Intersection of Hippo/YAP and Wnt/beta-catenin signaling pathways. <u>Acta</u> Biochim Biophys Sin (Shanghai) 45, 71, 2013.

- 18. Heallen, T., Zhang, M., Wang, J., Bonilla-Claudio, M., Klysik, E., Johnson, R.L., and Martin, J.F. Hippo pathway inhibits Wnt signaling to restrain cardiomyocyte proliferation and heart size. Science **332**, 458, 2011.
- Azzolin, L., Panciera, T., Soligo, S., Enzo, E., Bicciato, S., Dupont, S., Bresolin, S., Frasson, C., Basso, G., Guzzardo, V., Fassina, A., Cordenonsi, M., and Piccolo, S. YAP/TAZ incorporation in the beta-catenin destruction complex orchestrates the Wnt response. Cell 158, 157, 2014.
- Park, H.W., Kim, Y.C., Yu, B., Moroishi, T., Mo, J.S., Plouffe, S.W., Meng, Z., Lin, K.C., Yu, F.X., Alexander, C.M., Wang, C.Y., and Guan, K.L. Alternative Wnt signaling activates YAP/TAZ. Cell 162, 780, 2015.
- Bratt-Leal, A.M., Nguyen, A.H., Hammersmith, K.A., Singh, A., and McDevitt, T.C. A microparticle approach to morphogen delivery within pluripotent stem cell aggregates. Biomaterials 34, 7227, 2013.
- Baraniak, P.R., Cooke, M.T., Saeed, R., Kinney, M.A., Fridley, K.M., and McDevitt, T.C. Stiffening of human mesenchymal stem cell spheroid microenvironments induced by incorporation of gelatin microparticles. <u>J Mech</u> Behav Biomed Mater 11, 63, 2012.
- 23. DeVolder, R.J., Kim, I.W., Kim, E.S., and Kong, H. Modulating the rigidity and mineralization of collagen gels using poly(lactic-co-glycolic acid) microparticles. <u>Tissue</u> Eng Part A **18**, 1642, 2012.
- Si-Tayeb, K., Noto, F.K., Sepac, A., Sedlic, F., Bosnjak, Z.J., Lough, J.W., and Duncan, S.A. Generation of human induced pluripotent stem cells by simple transient transfection of plasmid DNA encoding reprogramming factors. BMC Dev Biol 10, 81, 2010.
- Si-Tayeb, K., Noto, F.K., Nagaoka, M., Li, J., Battle, M.A., Duris, C., North, P.E., Dalton, S., and Duncan, S.A. Highly efficient generation of human hepatocyte-like cells from induced pluripotent stem cells. <u>Hepatology</u> 51, 297, 2010.
- Yan, Y., Martin, L., Bosco, D., Bundy, J., Nowakowski, R., Sang, Q.X., and Li, Y. Differential effects of acellular embryonic matrices on pluripotent stem cell expansion and neural differentiation. Biomaterials 73, 231, 2015.
- 27. Yan, Y., Bejoy, J., Xia, J., Guan, J., Zhou, Y., and Li, Y. Neural patterning of human induced pluripotent stem cells in 3-D cultures for studying biomolecule-directed differential cellular responses. Acta Biomater **42**, 114, 2016.
- Zhang, D., Giese, M.L., Prukop, S.L., and Grunlan, M.A. PCL-based shape memory polymers with variable PDMS soft segment lengths. <u>J Polym Sci A Polym Chem</u> 49, 754, 2011.
- Zhang, D., Petersen, K.M., and Grunlan, M.A. Inorganicorganic shape memory polymer (SMP) foams with highly tunable properties. <u>ACS Appl Mater Interfaces</u> 5, 186, 2013.
- Song, L. PCL-PDMS-PCL copolymer-based microspheres mediate cardiovascular differentiation from embryonic stem cells [M.S. thesis]. Florida State University, 2015.
- 31. Cai, T., Li, M., Zhang, B., Neoh, K.-G., and Kang, E.-T. Hyperbranched polycaprolactone-click-poly(N-vinylcaprolactam) amphiphilic copolymers and their applications as temperature-responsive membranes. J Mater Chem B 2, 814, 2014.
- Song, L., Wang, K., Li, Y., and Yang, Y. Nanotopography promoted neuronal differentiation of human induced pluripotent stem cells. <u>Colloids Surf B Biointerfaces</u> 148, 49, 2016.
- 33. Sart, S., Calixto Bejarano, F., Baird, M.A., Yan, Y., Rosenberg, J.T., Ma, T., Grant, S.C., and Li, Y. Intracellular

labeling of mouse embryonic stem cell-derived neural progenitor aggregates with micron-sized particles of iron oxide. Cytotherapy **17**, 98, 2015.

- Sart, S., Ma, T., and Li, Y. Extracellular matrices decellularized from embryonic stem cells maintained their structure and signaling specificity. <u>Tissue Eng Part A</u> 20, 54, 2014.
- 35. Johnson, R., and Halder, G. The two faces of Hippo: targeting the Hippo pathway for regenerative medicine and cancer treatment. Nat Rev Drug Discov 13, 63, 2014.
- 36. ten Berge, D., Koole, W., Fuerer, C., Fish, M., Eroglu, E., and Nusse, R. Wnt signaling mediates self-organization and axis formation in embryoid bodies. <u>Cell Stem Cell</u> **3**, 508, 2008.
- Nicoleau, C., Varela, C., Bonnefond, C., Maury, Y., Bugi, A., Aubry, L., Viegas, P., Bourgois-Rocha, F., Peschanski, M., and Perrier, A.L. Embryonic stem cells neural differentiation qualifies the role of Wnt/beta-Catenin signals in human telencephalic specification and regionalization. Stem Cells 31, 1763, 2013.
- 38. Bejoy, J., Song, L., and Li, Y. Wnt-YAP interactions in the neural fate of human pluripotent stem cells and the implications for neural organoid formation. <u>Organogenesis</u> 12, 1, 2016.
- 39. van den Ameele, J., Tiberi, L., Vanderhaeghen, P., and Espuny-Camacho, I. Thinking out of the dish: what to learn about cortical development using pluripotent stem cells. Trends Neurosci **37**, 334, 2014.
- Lippmann, E.S., Williams, C.E., Ruhl, D.A., Estevez-Silva, M.C., Chapman, E.R., Coon, J.J., and Ashton, R.S. Deterministic HOX patterning in human pluripotent stem cellderived neuroectoderm. Stem Cell Reports 4, 632, 2015.
- Dupont, S., Morsut, L., Aragona, M., Enzo, E., Giulitti, S., Cordenonsi, M., Zanconato, F., Le Digabel, J., Forcato, M., Bicciato, S., Elvassore, N., and Piccolo, S. Role of YAP/ TAZ in mechanotransduction. Nature 474, 179, 2011.
- Yang, C., Tibbitt, M.W., Basta, L., and Anseth, K.S. Mechanical memory and dosing influence stem cell fate. <u>Nat Mater</u> 13, 645, 2014.
- 43. Zhao, B., Tumaneng, K., and Guan, K.L. The Hippo pathway in organ size control, tissue regeneration and stem cell self-renewal. Nat Cell Biol 13, 877, 2011.
- Hsiao, C., Lampe, M., Nillasithanukroh, S., Han, W., Lian, X., Palecek, S.P. Human pluripotent stem cell culture density modulates YAP signaling. <u>Biotechnol J</u> 11, 662, 2016.
- Sun, Y., Yong, K.M., Villa-Diaz, L.G., Zhang, X., Chen, W., Philson, R., Weng, S., Xu, H., Krebsbach, P.H., and Fu, J. Hippo/YAP-mediated rigidity-dependent motor neuron differentiation of human pluripotent stem cells. <u>Nat Mater</u> 13, 599, 2014.
- 46. Musah, S., Wrighton, P.J., Zaltsman, Y., Zhong, X., Zorn, S., Parlato, M.B., Hsiao, C., Palecek, S.P., Chang, Q.,

- Murphy, W.L., and Kiessling, L.L. Substratum-induced differentiation of human pluripotent stem cells reveals the coactivator YAP is a potent regulator of neuronal specification. Proc Natl Acad Sci U S A 111, 13805, 2014.
- Guo, X., and Zhao, B. Integration of mechanical and chemical signals by YAP and TAZ transcription coactivators. Cell Biosci 3, 33, 2013.
- Wada, K., Itoga, K., Okano, T., Yonemura, S., and Sasaki, H. Hippo pathway regulation by cell morphology and stress fibers. Development 138, 3907, 2011.
- Ohgushi, M., Minaguchi, M., and Sasai, Y. Rho-signalingdirected YAP/TAZ activity underlies the long-term survival and expansion of human embryonic stem cells. <u>Cell Stem</u> Cell 17, 448, 2015.
- 50. Salerno, A., Levato, R., Mateos-Timoneda, M.A., Engel, E., Netti, P.A., and Planell, J.A. Modular polylactic acid microparticle-based scaffolds prepared via microfluidic emulsion/solvent displacement process: fabrication, characterization, and in vitro mesenchymal stem cells interaction study. J Biomed Mater Res A 101, 720, 2013.
- 51. Bratt-Leal, A.M., Carpenedo, R.L., Ungrin, M.D., Zandstra, P.W., and McDevitt, T.C. Incorporation of biomaterials in multicellular aggregates modulates pluripotent stem cell differentiation. Biomaterials **32**, 48, 2011.
- Luciani, A., Coccoli, V., Orsi, S., Ambrosio, L., and Netti,
 P.A. PCL microspheres based functional scaffolds by bottomup approach with predefined microstructural properties and release profiles. Biomaterials 29, 4800, 2008.
- 53. Nguyen, A.H., Wang, Y., White, D.E., Platt, M.O., and McDevitt, T.C. MMP-mediated mesenchymal morphogenesis of pluripotent stem cell aggregates stimulated by gelatin methacrylate microparticle incorporation. <u>Biomaterials</u> **76**, 66, 2015.
- Sasai, Y. Next-generation regenerative medicine: organogenesis from stem cells in 3D culture. <u>Cell Stem Cell</u> 12, 520, 2013.
- Gjorevski, N., Ranga, A., and Lutolf, M.P. Bioengineering approaches to guide stem cell-based organogenesis. <u>Development</u> 141, 1794, 2014.

Address correspondence to:
Yan Li, PhD
Department of Chemical and Biomedical Engineering
FAMU-FSU College of Engineering
Florida State University
2525 Pottsdamer Street
Tallahassee, FL 32310

E-mail: yli@eng.fsu.edu

Received: March 31, 2017 Accepted: July 7, 2017 Online Publication Date: August 31, 2017

This article has been cited by:

- 1. Julie Bejoy, Liqing Song, Zhe Wang, Qing-Xiang Sang, Yi Zhou, Yan Li. 2018. Neuroprotective Activities of Heparin, Heparinase III, and Hyaluronic Acid on the Aβ42-Treated Forebrain Spheroids Derived from Human Stem Cells. ACS Biomaterials Science & Engineering 4:8, 2922-2933. [Crossref]
- 2. Yuanwei Yan, Liqing Song, Julie Bejoy, Jing Zhao, Takahisa Kanekiyo, Guojun Bu, Yi Zhou, Yan Li. 2018. Modeling Neurodegenerative Microenvironment Using Cortical Organoids Derived from Human Stem Cells. *Tissue Engineering Part A* 24:13-14, 1125-1137. [Crossref]
- 3. Liqing Song, Mohammad Faisal Ahmed, Yan Li, Changchun Zeng, Yan Li. 2018. Vascular differentiation from pluripotent stem cells in 3-D auxetic scaffolds. *Journal of Tissue Engineering and Regenerative Medicine* 12:7, 1679-1689. [Crossref]
- 4. Song Liqing, Tsai Ang-Chen, Yuan Xuegang, Bejoy Julie, Sart Sébastien, Ma Teng, Li Yan. 2018. Neural Differentiation of Spheroids Derived from Human Induced Pluripotent Stem Cells–Mesenchymal Stem Cells Coculture. *Tissue Engineering Part A* 24:11-12, 915-929. [Abstract] [Full Text] [PDF] [PDF Plus] [Supplementary Material]
- 5. Song Liqing, Ahmed Mohammad Faisel, Li Yan, Bejoy Julie, Zeng Changchun, Li Yan. 2017. PCL-PDMS-PCL Copolymer-Based Microspheres Mediate Cardiovascular Differentiation from Embryonic Stem Cells. *Tissue Engineering Part C: Methods* 23:10, 627-640. [Abstract] [Full Text] [PDF] [PDF Plus] [Supplementary Material]